Inorganic Chemistry
Article

Inorg. Chem. **2009**, *48*, 8317–8324 **8317**
DOI: 10.1021/ic900939c

A High-Spin Organometallic Fe−S Compound: Structural and Mössbauer Spectroscopic Studies of [Phenyltris((*tert*-butylthio)methyl)borate]Fe(Me)

Codrina V. Popescu,*,† Michael T. Mock,‡ Sebastian A. Stoian,§ William G. Dougherty,‡ Glenn P. A. Yap,‡ and Charles G. Riordan*,‡

†*Department of Chemistry, Ursinus College, Collegeville, Pennsylvania 19426,* ‡*Department of Chemistry and Biochemistry, University of Delaware, Newark, Delaware 19716, and* §*Department of Chemistry, Carnegie Mellon University, Pittsburgh, Pennsylvania, 15213*

Received May 13, 2009

The synthesis and structure of the pseudotetrahedral, sulfur-rich, high-spin organoiron(II) [phenyltris((*tert*-butylthio)methyl)borate]Fe(Me), [PhTt^{tBu}]Fe(Me), **1**, are reported. Low-temperature Mössbauer spectroscopic studies reveal an isomer shift of δ = 0.60(3) mm/s and ΔE_Q = 0.00(1) mm/s and an S = 2 ground multiplet with a negative zero-field splitting, D = −33(3) cm^{-1}, $E/D \approx 0.01$. The small separation of the ground doublet, $\Delta \approx 0.01$ cm^{-1}, allows for observation of X-band EPR signals at $g_{eff} \approx 10$ (g_z = 2.6, $g_{x,y}$ = 2.00). The relatively large negative zero-field splitting and a highly anisotropic magnetic hyperfine tensor, containing a large orbital *z* component, {−10(4), −10(4), +33.8(2) MHz}, are concordant with the presence of unquenched orbital angular momentum. Density functional theory (DFT) calculations predict that the lowest-lying orbitals have predominantly d_{xy}- and $d_{x^2-y^2}$-like character, separated by an energy gap small enough to allow mixing through spin−orbit coupling, to generate a negative zero-field splitting, consistent with the experimental observations. The experimental and DFT-calculated isomer shifts are in good agreement (δ(calcd) = 0.5 mm/s). The unusual (for a high-spin ferrous site) null electric field gradients can be qualitatively explained in the frame of the spin−orbit coupling mixing. The very small Fermi contact component of the magnetic hyperfine tensor (A_{FC}(exp) = −9 MHz) is not well described by the DFT approach (A_{FC}(calcd) = +2 MHz). To our knowledge, this is the first study of a sulfur-coordinated high-spin organoiron(II) complex.

1. Introduction

Iron−sulfur clusters of various complexities are ubiquitous in living organisms. The basic structural module of these units is a high-spin $Fe^{(II)}/Fe^{(III)}$ site coordinated by four sulfur donors in a pseudotetrahedral arrangement. Three-coordinate high-spin $Fe^{(II)}$ sites are also known, but they are uncommon.[1−4] Rubredoxin sites contain four Cys donors, whereas higher-nuclearity clusters possess a combination of Cys and sulfide (S^{2-}) ligands. Because of its biological importance, this type of site has been thoroughly studied in the isolated proteins and model complexes with a variety of ligand donor sets, for example, four cysteine-derived sulfur donors in rubredoxin, 3S(Cys) + 1O(Ser) donors in rubredoxin variants,[5] or 2S(Cys) and 2N(His) in Rieske proteins.[6] Thus, the electronic structure of pseudotetrahedral ferrous complexes is well investigated.[7−9] A large change in the bonding and hyperfine interactions of the four-coordinate ferrous ion is caused by replacing a sulfur donor with an alkyl ligand, which yields a coordinatively unsaturated high-spin organoiron complex. Because coordinatively unsaturated alkyl complexes are key intermediates in catalytic and stoichiometric couplings, such as olefin polymerizations, it is important to characterize their structure, spectroscopy, and reactivity.[10−12] These unsaturated coordination environments (of two, three, or four ligands) favor high-spin configurations for first-row transition series organometallics, leading to unusual electronic structures.[13−17] In contrast to

*To whom correspondence should be addressed. E-mail: cpopescu@ursinus.edu (C.V.P.), riordan@udel.edu (C.G.R.).

(1) Chan, M. K.; Kim, J.; Rees, D. C. *Science* **1993**, *260*, 792–794.
(2) Peters, J. W.; Stowell, M. H. B.; Soltis, S. M.; Finnegan, M. G.; Johnson, M. K.; Rees, D. C. *Biochemistry* **1997**, *36*, 1181–1187.
(3) MacDonnell, F. M.; Ruhlandt-Senge, K.; Ellison, J. J.; Holm, R. H.; Power, P. P. *Inorg. Chem.* **1995**, *34*, 1815–1822.
(4) Smith, J. M.; Lachicotte, R. J.; Holland, P. L. *Chem. Commun.* **2001**, 1542–43.
(5) Yoo, S. J.; Meyer, J.; Achim, C.; Peterson, J.; Hendrich, M. P.; Münck, E. *J. Biol. Inorg. Chem.* **2000**, *5*, 475–487.
(6) Pikus, J.; Studts, J.; Achim, C.; Kauffmann, K.; Münck, E.; Steffan, R.; McClay, K.; Fox, B. G. *Biochemistry* **1996**, 9106–9119.
(7) Coucouvanis, D. *J. Am. Chem. Soc.* **1981**, *103*, 3350–3362.
(8) Gebhard, M. S.; Koch, S. A.; Millar, M.; Devlin, F. J.; Stephens, P. J.; Solomon, E. I. *J. Am. Chem. Soc.* **1991**, *113*, 1640–49.
(9) Werth, M. T. *Inorg. Chem.* **1989**, *28*, 1537–61.
(10) Akita, M. *J. Organomet. Chem.* **2004**, *689*, 4540–4551.
(11) Shirasawa, N.; Nguyet, T. T.; Hikichi, S.; Moro-oka, Y.; Akita, M. *Organometallics* **2001**, *20*, 3582–3598.
(12) Small, B. L.; Brookhart, M.; Bennett, A. M. A. *J. Am. Chem. Soc.* **1998**, *120*, 4049–4050.
(13) Brunker, T. J.; Barlow, S. *Chem. Commun.* **2001**, 2052–2053.

Published on Web 07/30/2009

the vast literature detailing low-spin organoiron complexes that obey the 18-electron rule, the electronic structure of high-spin organoiron complexes has remained largely unexplored. One notable exception is the spectroscopic and theoretical study of a trigonal methyliron(II) complex supported by a β-diketiminate ligand, LFe(Me) (L = β-diketiminate).[18] Andres et al. explored the electronic structure and bonding in this complex by Mössbauer, electron paramagnetic resonance (EPR), and theoretical studies. Their results revealed large unquenched orbital angular momentum in one spatial direction (namely, on the axis perpendicular to the β-diketiminate plane) due to the presence of low-lying excited orbital states. A closer examination, by the same group, of the electronic structure of additional two- and planar three-coordinate $Fe^{(II)}$ and $Fe^{(I)}$ compounds established that the unquenched orbital angular momentum is a common feature of this family of iron compounds. This unquenching phenomenon generates ground states, which are pseudodoublets for $Fe^{(II)}$ and Kramers doublets for $Fe^{(I)}$, that exhibit uniaxial magnetic behavior with large effective g values ($g_{eff} \approx 11.4$ for the [(β-diketiminate)$Fe^{(II)}$Me])[18] and large internal magnetic fields along the spin quantization axis.[19,20] Another unusual feature of the planar ferrous β-diketiminate complexes is their small quadrupole splitting ($1.11 < |\Delta E_Q| < 1.74$ mm/s, for the [(β-diketiminate)$Fe^{(II)}$L] series, L = NH*t*Bu, NHTol, Cl, CH_3), shown to be caused by ligand contributions to the electric field gradients (EFGs) and associated with the planarity of the complex, rather than the coordinated alkyl.[18,21]

We report the synthesis and characterization of the C_3-symmetric complex [PhTt^{tBu}]Fe(Me), **1** (PhTt^{tBu} = $C_6H_5B(CH_2SC(CH_3)_3)_3$), including crystallographic, Mössbauer, and EPR spectroscopic studies. To our knowledge, this is the first report of a sulfur-ligated, organoiron complex with a high-spin configuration. According to the data presented here, **1** is a 14-electron, high-spin ferrous complex, in which the symmetry and alkyl coordination produce an orbital ground state (consisting predominantly of d_{xy} assuming the z axis along the Fe−C bond, Figure 1) that mixes through spin−orbit coupling with the next state ($d_{x^2-y^2}$-like), generating a relatively large and negative zero-field splitting (ZFS), a large magnetic moment along the z axis, and a ground spin state with uniaxial magnetic properties.

2. Materials and Experimental Methods

Due to the air and moisture sensitivity of complex **1**, all manipulations were performed under a nitrogen atmosphere employing solvents predried via passage through columns of activated alumina[22] with oxygen subsequently removed via a nitrogen purge.

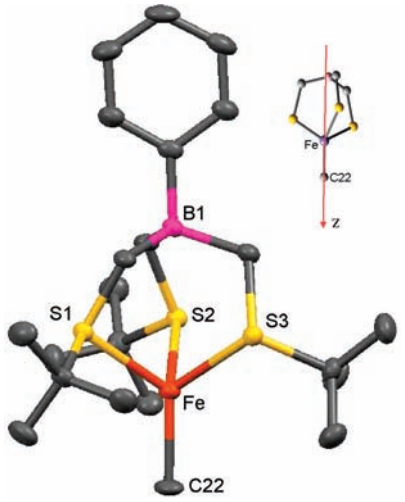

Figure 1. Molecular structure of [PhTt^{tBu}]Fe(Me) (**1**) with thermal ellipsoids drawn to 30% probability (H atoms not shown). Inset: A molecular model (truncated for clarity) showing the z axis used for spectroscopic and DFT calculations.

a. Synthesis of 1. MeMgBr (3.0 M in ethyl ether, 55 μL, 0.15 mmol) was added to a vial via syringe. This solution was diluted with 10 mL of ethyl ether, and 1,4-dioxane was added dropwise precipitating $MgCl_2$. The cloudy mixture was added dropwise to a stirring 1,4-dioxane solution (30 mL) of {[PhTt^{tBu}]FeCl}$_2$[23] (0.075 g, 0.15 mmol), producing a cloudy yellow solution. The mixture was stirred for 10 min and then filtered through Celite. The solvent was removed in vacuo, affording a light brown solid that was extracted with pentane (2 × 3 mL) and dried under a vacuum, yielding a yellow solid. Yellow blocks of **1** were grown by slow evaporation of a concentrated pentane solution. Yield: 0.041 g, 72%. ^{1}H NMR (C_6D_6): δ 42.9 (s, *m*-(C_6H_5)B), 20.2 (s, *o*-(C_6H_5)B), 18.7 (s, *p*-(C_6H_5)B), −26.4 (br, $(CH_3)_3$S). UV−vis (THF), λ_{max} (ε, M^{-1} cm^{-1}): 323 (1100). Anal. Calcd for $C_{22}H_{41}BFeS_3$: C, 56.41; H, 8.82. Found: C, 56.04; H, 8.89. The magnetic moment of **1** was measured in solution by the Evans method,[24] μ_{eff} (C_6D_6) = 5.1(2) μ_B.

b. X-Ray Diffraction. Crystal data collection and refinement parameters are given in Table 1. Yellow blocks of **1** were grown by slow evaporation of a concentrated pentane solution. Crystals were mounted using viscous oil on glass fibers and cooled to the data collection temperature. Data were collected on a Bruker-AXS APEX CCD diffractometer with graphite-monochromated Mo Kα radiation (λ = 0.71073 Å). Unit cell parameters were obtained from 60 data frames, 0.3° ω, from three different sections of the Ewald sphere. The systematic absences in the diffraction data are uniquely consistent with the monoclinic space group, $P2_1/n$. The data sets were treated with SADABS absorption corrections based on redundant multiscan data.[25] The structure was solved using direct methods and refined with full-matrix, least-squares procedures on F^2. All non-hydrogen atoms were refined with anisotropic displacement parameters. All hydrogen atoms were treated as idealized contributions. Structure factors are contained in the SHELXTL 6.12 program library.[25]

c. Mössbauer and EPR Spectroscopy. Mössbauer samples were prepared in a Vacuum Atmospheres glovebox by stirring

(14) Daida, E. J.; Peters, J. C. *Inorg. Chem.* **2004**, *43*, 7474–7485.
(15) DuPont, J. A.; Coxey, M. B.; Schebler, P. J.; Incarvito, C. D.; Dougherty, W. G.; Yap, G. P. A.; Rheingold, A. L.; Riordan, C. G. *Organometallics* **2007**, *26*, 971–979.
(16) Kisko, J. L.; Hascall, T.; Parkin, G. *J. Am. Chem. Soc.* **1998**, *120*, 10561–10562.
(17) Reiff, W. M.; Schulz, C. E.; Whangbo, M.-H.; Seo, J. I.; Lee, Y. S.; Potratz, G. R.; Spicer, C. W.; Girolami, G. S. *J. Am. Chem. Soc.* **2009**, *131*, 404–405.
(18) Andres, H.; Bominaar, E. L.; Smith, J. M.; Eckert, N. A.; Holland, P. L.; Münck, E. *J. Am. Chem. Soc.* **2002**, *124*, 3012–3025.
(19) Stoian, S. A.; Vela, J.; Smith, J. M.; Sadique, A. R.; Holland, P. L.; Münck, E.; Bominaar, E. L. *J. Am. Chem. Soc.* **2006**, *128*, 10181–10192.
(20) Stoian, S. A.; Yu, Y.; Smith, J. M.; Holland, P. L.; Bominaar, E. L.; Münck, E. *Inorg. Chem.* **2005**, *44*, 4915–4922.
(21) Zhang, Y.; Oldfield, E. *J. Phys. Chem. B* **2003**, *107*, 7180–7188.
(22) Pangborn, A. B.; Giardello, M. A.; Grubbs, R. H.; Rosen, R. K.; Timmers, F. J. *Organometallics* **1996**, *15*, 1518–1520.
(23) Mock, M. T.; Popescu, C. V.; Yap, G. P. A.; Dougherty, W. G.; Riordan, C. G. *Inorg. Chem.* **2008**, *47*, 1889–1891.
(24) Evans, D. F. *J. Chem. Soc.* **2003**, 1959.
(25) Sheldrick, G. M. *Acta Crystallogr., Sect. A* **2008**, *64*, 112–122.

the microcrystalline powder in degassed mineral oil in 1 mL plastic sample cells and then freezing the sample in liquid nitrogen. Mössbauer spectra were recorded on three independent preparations of compound **1**, on two constant acceleration spectrometers. Low-field (0.03 T), variable-temperature (4.5−200 K) Mössbauer spectra were recorded on a closed-cycle refrigerator spectrometer, model CCR4K, equipped with a 0.03 T permanent magnet, which maintains temperatures between 4.5 and 300 K (SeeCo.us). High-field, variable-temperature spectra were recorded at Carnegie Mellon University, on a spectrometer cooled with liquid helium, equipped with a superconducting magnet at cryogenic temperatures, between 1.5 and 250 K. Mössbauer spectra were analyzed using the software WMOSS (See Co. formerly Web Research, Edina, MN).

EPR spectroscopy was performed on a Bruker ESP 300 spectrometer, equipped with an ESR 910 helium continuous flow cryostat and Oxford temperature controller, at Carnegie Mellon University. The analysis of EPR spectra was done with the SpinCount software written by Dr. M. P. Hendrich (Carnegie Mellon University). Both Mössbauer and EPR measurements were conducted on a microcrystalline powder sample dispersed in nujol and on a frozen toluene solution.

d. Density Functional Theory Calculations. Density functional theory (DFT) calculations and geometry optimizations were performed with the Gaussian 03 software,[26] using the B3LYP hybrid functional and the 6-311G basis set. Details of the calculations are available in the Supporting Information.

3. Results

3.1. Synthesis and Spectroscopic Characterization of 1. Complex **1** was obtained in good yield via the action of *in situ* prepared Me_2Mg on $\{[PhTt^{tBu}]FeCl\}_2$.[23] Previously, we found this approach successful for the synthesis of the analogous cobalt derivatives, $[PhTt^{tBu}]Co(R)$ (R = Me, Et, Bn, Ph, allyl).[15] Complex **1** was isolated as a yellow, air-sensitive, microcrystalline solid. The ^1H NMR spectrum shows paramagnetically dispersed resonances consistent with its high-spin state, $S = 2$ (vide infra). The phenyl signals are shifted downfield, whereas the *tert*-butyl resonance is significantly upfield shifted, $\delta = -26.4$. The methyliron protons are not detected, presumably due to efficient relaxation caused by their proximity to the iron center or because the signal is shifted beyond our observation window. Parkin's four-coordinate $[PhTp^{tBu}]Fe(Me)$ complex[16] (phenyltris(3-*tert*-butylpyrazolyl)borato iron methyl)) exhibited a ^2H NMR signal at $\delta = 1453$ for the d_3 isotopomer.

3.2. Molecular Structure of 1. The molecular structure of **1**, determined by X-ray diffraction, is shown in Figure 1 with selected metric parameters contained in Table 2.

Table 1. Crystallographic Data for **1**

	$[PhTt^{tBu}]Fe(Me)$
empirical formula	$C_{22}H_{41}BFeS_3$
fw	468.39
color, habit	yellow, blocks
cryst syst	monoclinic
space group	$P2_1/n$
a, Å	9.669(9)
b, Å	21.72(2)
c, Å	12.382(11)
α, deg	90
β, deg	98.975(17)
γ, deg	90
V(Å^3)	2569(4)
λ, Å (Mo, Kα)	0.71073
Z	4
density (g/cm^3)	1.211
temperature (K)	120(2)
2*θ* range, deg	1.91 − 28.24
μ(Mo, Kα), mm^{-1}	0.836
R(F), *Rw*(F)[a]	0.0411, 0.1066

[a] Quantity minimized = $R(wF^2) = \sum[w(F_o^2 - F_c^2)^2]/\sum[(wF_o^2)^2]^{1/2}$; $R = \sum\Delta/\sum(F_o)$, $\Delta = |(F_o - F_c)|$, $w = 1/[\sigma^2(F_o^2) + (aP)^2 + bP]$, $P = [2F_c^2 + \mathrm{Max}(F_o,0)]/3$.

Table 2. Selected Bond Lengths (Å) and Angles (deg) for **1**

	length (Å)		angle (deg)
Fe−S1	2.402(2)	S1−Fe−C22	121.98(8)
Fe−S2	2.409(2)	S2−Fe−C22	123.52(8)
Fe−S3	2.416(2)	S3−Fe−C22	122.43(1)
Fe−C22	2.034(3)	S1−Fe−S2	93.90(7)
		S1−Fe−S3	93.24(5)
		S2−Fe−S3	93.77(6)
		B···Fe−C22	179.1

Complex **1** is isomorphous with the cobalt analogue, $[PhTt^{tBu}]Co(Me)$.[15] The structure reveals an approximate C_3 symmetry with the Fe−Me along a noncrystallographically imposed 3-fold axis; the B···Fe−C angle is 179.1°. The relatively long iron−ligand distances are consistent with its high-spin ferrous formulation. The Fe−S distances are all quite similar and average to 2.41 Å. The S−Fe−S angles fall within a narrow range averaging to 93.64°. The Fe−C bond distance is 2.034(3) Å, which is in the range, 2.001−2.0956 Å, of the small number of structurally characterized four-coordinate iron-methyl complexes (Table 3).

3.3. Mössbauer and EPR Spectroscopy of 1. The Mössbauer spectrum of polycrystalline **1** in nujol at 5 K consists of a broad singlet with $\delta = 0.60(3)$ mm/s and quadrupole splitting, $\Delta E_Q = 0.00(1)$ mm/s. The isomer shift of **1** is at the lower end of the range expected for ferrous compounds with pseudotetrahedral, sulfur-rich coordination, which typically have isomer shifts between 0.6 and 0.7 mm/s.[5,27] A drop in isomer shift indicates an increase in the s-electron density at the nucleus, which is consistent with the substitution of a S donor with a C donor.[28−30] No direct comparisons of the isomer shift are appropriate,

(26) Frisch, M. J.; Trucks, G. W.; Schlegel, H. B.; Scuseria, G. E.; Robb, M. A.; Cheeseman, J. R.; Montgomery, J. A., Jr.; Vreven, T.; Kudin, K. N.; Burant, J. C.; Millam, J. M.; Iyengar, S. S.; Tomasi, J.; Barone, V.; Mennucci, B.; Cossi, M.; Scalmani, G.; Rega, N.; Petersson, G. A.; Nakatsuji, H.; Hada, M.; Ehara, M.; Toyota, K.; Fukuda, R.; Hasegawa, J.; Ishida, M.; Nakajima, T.; Honda, Y.; Kitao, O.; Nakai, H.; Klene, M.; Li, X.; Knox, J. E.; Hratchian, H. P.; Cross, J. B.; Adamo, C.; Jaramillo, J.; Gomperts, R.; Stratmann, R. E.; Yazyev, O.; Austin, A. J.; Cammi, R.; Pomelli, C.; Ochterski, J. W.; Ayala, P. Y.; Morokuma, K.; Voth, G. A.; Salvador, P.; Dannenberg, J. J.; Zakrzewski, V. G.; Dapprich, S.; Daniels, A. D.; Strain, M. C.; Farkas, O.; Malick, D. K.; Rabuck, A. D.; Raghavachari, K.; Foresman, J. B.; Ortiz, J. V.; Cui, Q.; Baboul, A. G.; Clifford, S.; Cioslowski, J.; Stefanov, B. B.; Liu, G.; Liashenko, A.; Piskorz, P.; Komaromi, I.; Martin, R. L.; Fox, D. J.; Keith, T.; Al-Laham, M. A.; Peng, C. Y.; Nanayakkara, A.; Challacombe, M.; Gill, P. M. W.; Johnson, B.; Chen, W.; Wong, M. W.; Gonzalez, C.; Pople, J. A. *Gaussian 03*, revision C.2; Gaussian, Inc.: Wallingford, CT, 2004.

(27) Münck, E. *Aspects of ^{57}Fe Mössbauer Spectroscopy*; Que, L., Jr. Ed.; University Science Books: Sausalito, CA, 2000.

(28) Goldanskii, V. I.; Herber, R. *Chemical Applications of Mössbauer Spectroscopy*; Academic Press: New York, 1968.

(29) Greenwood, N. N.; Gibb, T. C. *Mössbauer Spectroscopy*; 1971 ed.; Chapman Hall Ltd.: London, 1971.

(30) Gutlich, P.; Link, R.; Trautwein, A. *Mössbauer Spectroscopy and Transition Metal Chemistry*; Springer Verlag: Berlin, 1979.

Table 3. List of Fe−Me Distances for Crystallographically Characterized, Four-Coordinate Complexes

	Fe−C, Å	reference
[PhTt^{tBu}]Fe(Me)	2.034(3)	this study
(tmeda)Fe(Me)(N(TMS)Ar)	2.084(6)	52
[PhTp^{tBu}]Fe(Me)	2.079(3)	16
(^{iPr}PDI)Fe(Me)	2.001(6)	53
[(^{iPr}PDI)Fe(Me)][Li(THF)$_4$]	2.015(8)	54
[PhBP$^{iPr}_3$]Fe(Me)	2.013(3)	14
[(Me$_4$Fe)(MeLi)][Li(OEt$_2$)]$_2$	2.095(4)[a]	55

[a] The other three Fe−C distances are longer, averaging 2.185(4) Å.

since there are no other alkyl ferrous four-coordinate complexes with sulfur ligation. The crystal structure, proton NMR characteristics, and the isomer shift of δ = 0.6 mm/s establish that **1** is a high-spin ferrous complex. The room-temperature magnetic moment of μ_{eff} = 5.1(2) μ_B[24] is slightly larger than the spin-only magnetic moment of $g[S(S+1)]^{1/2}$ = 4.90 μ_B, expected for an S = 2 configuration. (Note that, for the trigonal methyl complex studied in detail in Andres et al.,[18] the room-temperature magnetic moment was 5.5 μ_B.) At 150 and 200 K, the quadrupole splitting was the same as at 4.2 K. The spectra were interpreted using the spin Hamiltonian in eq 1, for the S = 2 multiplet, appended with the nuclear Hamiltonian, H_n (eq 2a), accounting for the magnetic hyperfine coupling, quadrupole interaction (eq 2b), and nuclear Zeeman interaction.

$$H_e = D\{S_z^2 - 2\} + E\{S_x^2 - S_y^2\} + \mu_B B\cdot\mathbf{g}\cdot S \quad (1)$$

$$H_n = \beta\mathbf{S}\cdot\mathbf{A}\cdot\mathbf{I} + H_Q - g_n\beta_n\mathbf{B}\cdot\mathbf{I} \quad (2a)$$

$$H_Q = \frac{eQVzz}{12}\left[3I_z^2 - \frac{15}{4} + \eta(I_x^2 - I_y^2)\right] \quad (2b)$$

In eqs 1 and 2, D and E are the zero-field splittings acting on the S = 2 multiplet of the high-spin Fe(II) ion, μ_B is the Bohr magneton, **g** is the **g** tensor, **A** is the magnetic hyperfine coupling tensor, and g_n and β_n are the nuclear gyromagnetic factor and nuclear magneton, respectively.

The spectrum of **1** in a 0.03 T applied field (Figure 2C) exhibits paramagnetic splittings, for a fraction of the molecules in the sample. A high-spin, ferrous, S = 2 complex may exhibit magnetic hyperfine structure in such a weak applied field, only if its zero-field splitting is negative, and the separation (Δ) of the ground doublet states, roughly described by $M_S = \pm 2$, is very small. (For derivations and details, see refs 5, 31, and 32.) The separation within the ground doublet is $\Delta \approx 3D(E/D)^2$; thus, it is anticipated that $E/D \ll 0.33$. A small separation of the ground doublet states is verified by the observation of the X-band EPR spectra in parallel and perpendicular modes (vide infra) and of magnetic broadening and incipient splitting, even in the Earth's magnetic field, of about 0.06 mT (Figure 2B, arrows).[33]

We have recorded the high-field spectra at 4 and 8 T at temperatures between 4.2 and 100 K. The procedure for

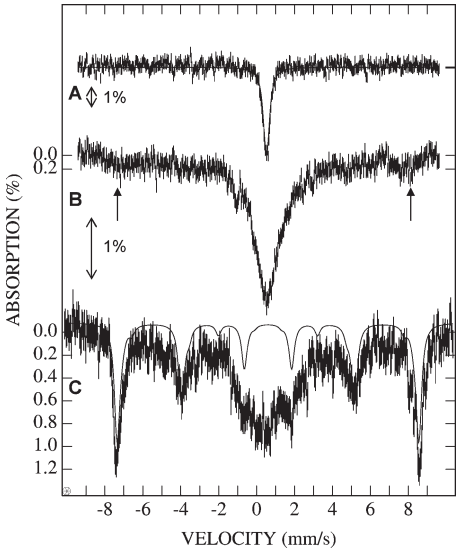

Figure 2. Low-field Mössbauer spectra of **1**: (A) 200 K, 0.03 T; (B) 5 K, 0 T; (C) 4.5 K, 0.03 T. The solid line in A is a spectral simulation with the parameters shown in Table 4, in the limit of fast relaxation of the electronic spin; the solid line in C is a simulation with the cited parameters, of 40% of the absorption, illustrating the determination of E/D from this spectrum (see also Figure S1, Supporting Information).

fitting variable-field spectra and extracting the Mössbauer parameters for ferrous ions, using eqs 1−2b, has been described previously.[31,34] The parameters that need to be determined from the Mössbauer spectra are the zero-field splitting parameters (D and E/D), the three principal components of the **A** tensor, A_i, and the **g** tensor, g_i (i = x, y, z), and the Euler angles between the field gradient and the zero-field splitting tensor, as well as the asymmetry parameter, η. In our case, since $\Delta E_Q \approx 0$ mm/s at all temperatures, η and the Euler angles are undetermined. The presence of a C_3 molecular symmetry axis ensures that all tensors share a common axis.

Inspection of the full Mössbauer data set affords several preliminary observations. First, the low-field spectrum in Figure 2C is composed of a six-line pattern, typical for a paramagnetic ground state, along with a broad absorption centered at δ = ~0.6 mm/s. This "diamagnetic" component can be explained by a distribution of the E/D parameter, with values in the range $0.01 < E/D < 0.1$. [The 4.5 K, 0.03 T spectrum in Figure 2 can be understood as a result of superimposing spectra of molecules with a distribution of E/D values in the range $0.01 < E/D < 0.1$. Simulations show that, starting with E/D ~ 0.02, one obtains absorption in the middle of the spectrum, corresponding to molecules that experience little to no internal field. A simulation obtained with four E/D values is shown in Figure S1 (Supporting Information). However, this is not the only mechanism to obtain no internal field in a population of molecules. We have found in the crystal structure of **1** three distinct intermolecular distances under 10 Å. These close contacts can give rise to spin dipolar couplings as large as 0.01 cm^{-1} (see below), which result in a spectral component around 0.6 mm/s. Nevertheless, the essential feature of the 0.03 T spectrum is the outermost splitting, which corresponds to

(31) Münck, E.; Surerus, K. K. *Methods Enzymol.* **1993**, *227*, 463–479.
(32) Zimmermann, R.; Spiering, H.; Ritter, G. *Chem. Phys.* **1974**, *4*, 133–141.
(33) U.S. Geological Survey. http://geomag.usgs.gov/charts (accessed 5/06/2009).
(34) Zimmermann, R.; Huynh, B. H.; Münck, E. *J. Chem. Phys.* **1978**, *69*, 5463–5467.

the internal field discussed, allowing determination of the upper limit of E/D.] Since **1** is an integer spin system, the paramagnetic component appears only in an applied field. In the absence of the magnetic field, the ground doublet is composed of states $\phi(\pm 2) = a^{+}|+2\rangle + a^{-}|-2\rangle$,[35,31] which are nonmagnetic and are separated by the zero-field parameter, Δ. When the Zeeman interaction overcomes Δ, that is, $\Delta \ll g_{\mathrm{eff}}\beta\mathrm{H}$, the $|-2\rangle$ state becomes the ground state and produces a magnetic Mössbauer spectrum. Since a significant fraction of the molecules in the powder sample show fully developed magnetic hyperfine splittings in the applied field of 0.03 T, the separation Δ is constrained to values lower than 0.03 cm^{-1}, which gives an upper boundary for E/D at 0.02. This type of simulation is illustrated in Figure 2C. Second, observation of the magnetic splittings at fields as low as 0.03 T indicates that the relaxation of the spin system is slow on the Mössbauer time scale, at 4.5 K. Third, comparison of spectra at 0.03 T and 4 and 8 T shows that the increase of the applied field causes the effective field at the nucleus ($B_{\mathrm{eff}} = B_{\mathrm{int}} + B_{\mathrm{app}}$) to increase; thus, B_{int} is positive for the ground state.

The 4.2 K spectra in applied fields for this compound show six-line patterns, indicating that the ground doublet has uniaxial magnetic behavior, with effective **g** values of $g_z > g_x, g_y$; thus, the quantization direction of the spin expectation value $\langle S\rangle$ is along the magnetic z direction.[27,36,37] The spectra in high applied magnetic field do not depend on E/D; thus, they would not be affected by the distribution observed at 0.03 T. Thus, the spectra depend primarily on g_z, A_z, and the zero-field splittings. From the 8 T spectrum at 4.2 K in Figure 3A, and using the E/D required by the 0.03 T spectrum, we can determine the internal field at the Fe nucleus along the z axis from the splitting of the outermost lines, $B_{\mathrm{int}} = (\langle S_i\rangle A_i)/(g_{\mathrm{n}}\beta_{\mathrm{n}}) \approx 492$ kG (where $i = x, y, z$), yielding $A_z \approx 246$ kG. In high fields, at 4.2 K, the Mössbauer spectra do not provide information about the internal fields along the x and y axes (hence, A_x and A_y), since the spin expectation values, $\langle S_x\rangle$ and $\langle S_y\rangle$, along the x and y axes, dictated by D and E/D, are very small. At a low temperature (4.2 K) and both 4 and 8 T (Figure 3), the spectra are not very sensitive to D and E/D; however, boundaries for D can be established. Fitting the spectra in Figure 3, and using the upper limit for E/D from the 0.03 T spectrum, we obtain $D < -25$ cm^{-1} and $0.01 \leq E/D \leq 0.02$.

At temperatures above 30 K, assuming fast electronic spin relaxation, the spectrum will reflect the population of higher states in the $S = 2$ multiplet, and the internal field will follow the Curie law,[20,27] given by $B_{\mathrm{int},z} = (2g_z\beta BA_z)/(kTg_{\mathrm{n}}\beta_{\mathrm{n}})$, where the A_z value is that determined from the 4.2 K spectra and the only unknown is g_z (k is the Boltzmann constant, and the other symbols carry the same meanings as defined above). Thus, from the total splitting of the 80 K spectrum (Figure 4), we can determine $g_z = 2.5$. Finally, simulations of the 100 K spectrum in Figure 4B place D around -30 cm^{-1}. The best fits to the entire data set were obtained with $-34\ \mathrm{cm}^{-1} \leq D \leq -30\ \mathrm{cm}^{-1}$, $0.01 \leq E/D \leq 0.02$, and $g_z = 2.5$, as given in Table 4.

(35) Sanakis, Y.; Power, P. P.; Stubna, A.; Münck, E. *Inorg. Chem.* **2002**, *41*, 2690–2696.
(36) Münck, E. *Methods Enzymol.* **1978**, *54*, 346–397.
(37) Münck, E. *The Porphyrins*; Academic Press: New York, 1979; Vol. *IV*, Chapter 8.

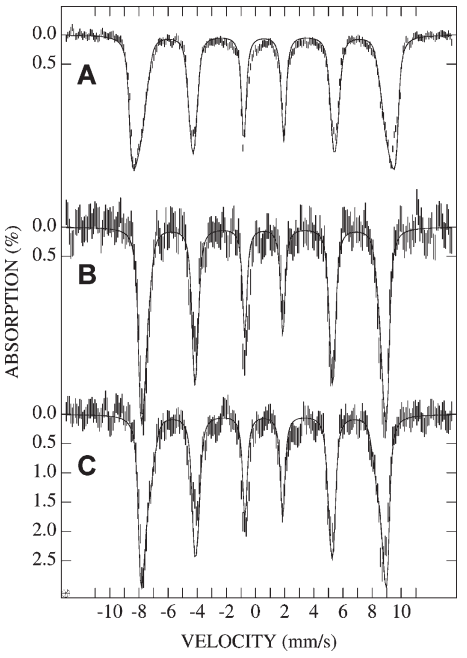

Figure 3. Mössbauer spectra of **1** in applied fields of 8 T, at 4.2 K (A), and 4 T, at 4.2 K (B) and 10 K (C). The solid lines are spectral fits obtained with the parameters in Table 4.

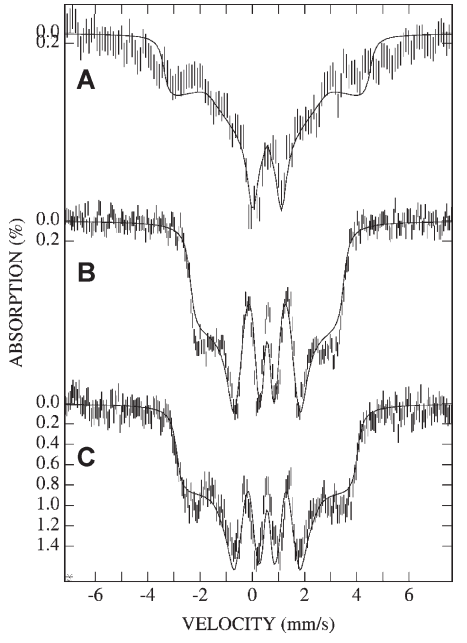

Figure 4. Mössbauer spectra of compound **1** recorded in (**A**) 4 T, at 30 K; (**B**) 8 T at 100 K; (**C**) 8 T at 80 K. The solid lines are fits to the spectra, with the parameters listed in Table 4.

Table 4. Spin-Hamiltonian Parameters Obtained from Mössbauer Spectroscopy for **1**

δ (mm/s)	ΔE_{Q} (mm/s)	D (cm^{-1})	E/D	A_x, A_y, A_z (MHz)	g_x, g_y, g_z
0.60(3)	0.0(1)	−33(3)	0.01	−10(4), −10(4), 33.8(2)	2.0, 2.0, 2.5(1)

In summary, the Mössbauer spectra are consistent with a high-spin ferrous ion with a negative zero-field splitting and a small separation of the ground doublet states,

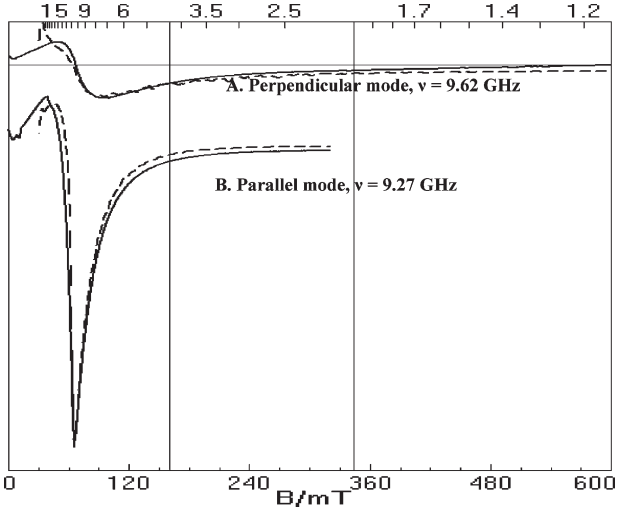

Figure 5. Perpendicular (**A**) and parallel (**B**) mode EPR spectra of a frozen toluene solution sample of **1**. The solid lines are the experimental spectra and dashed lines are simulations, obtained with $g_z = 2.6$, $D = -37$ cm^{-1}, $E/D = 0.029$, $\sigma(E/D) = 0.019$, and a packet line-width of 15 G. Spectra were collected at the microwave frequencies shown, with a 100 kHz modulation frequency, 1 mT modulation amplitude, and 0.2 mW microwave power.

which gives rise to low-temperature paramagnetism. The Mössbauer spectra show that the electronic system is uniaxial, allowing determination of the isomer shift, $\delta = 0.60(3)$ mm/s; quadrupole splitting, $\Delta E_Q = 0.00(1)$ mm/s; the largest component of the magnetic hyperfine tensor, $A_z = \pm 33.8(2)$ MHz; and fine structure parameters ($D = -33(3)$ cm^{-1}, $g_z = 2.5$, and $E/D \sim 0$). The upper limits of the other two components of the magnetic hyperfine tensor can be estimated as $A_{x,y} = -10(4)$ MHz.

3.4. EPR Spectroscopy. EPR spectra were recorded in both parallel and perpendicular modes, for a solution of **1** in toluene (Figure 5) and for a polycrystalline sample suspended in nujol (spectra shown in the Supporting Information). The frozen solution sample exhibits resonances near $g_{\text{eff}} \approx 10$ (parallel and perpendicular modes). The parameters of the EPR simulations are $D = -37(2)$ cm^{-1}, $E/D = 0.029$, and $g_z = 2.6$. While D is in satisfactory agreement with that obtained by Mössbauer spectroscopy, the rhombicity parameter is quite different from that required by the low-field Mössbauer spectrum (Figure 2). Given the heterogeneity of the powder sample and the sensitivity of the spectra to distance-dependent intermolecular interactions, we attribute the discrepancy to the difference in the intermolecular interactions between the powder sample (such as the Mössbauer sample) and a sample dissolved in toluene. The powder sample exhibits broad resonances starting near zero field, with minima at $g \approx 7$ (perpendicular mode) and $g \approx 8.7$ and $g \approx 12.8$ (parallel). It is known that shapes of integer-spin EPR spectra are complex and are sensitive to slight variations in molecular geometry.[38] The solution EPR signals are distinct from axial signals (which would have been expected according to the Mössbauer data), and to account for its line shape we used a Gaussian distribution for E/D, $\sigma(E/D)$. Distributions in ZFS and rhombicity parameters result from heterogeneities in the molecular geometry. Recently, the source of spectroscopic heterogeneity for a high-spin Fe$^{(II)}$ pseudotetrahedral complex was identified in a very narrow distribution of a molecular torsion angle.[39] It is possible that **1** has a similar distribution in molecular parameters, which was imperceptible in the crystal structure. The parameter set obtained from EPR is, overall, consistent with that from Mössbauer spectroscopy.

Table 5. Experimental and DFT Calculated Geometric Parameters for **1**, Derived Using the Full Molecule

distance/angle	experimental (Å)	calculated (Å)
Fe−C22	2.034(3)	2.021
Fe−S av.	2.412(2)	2.508
S−C(*tert*-butyl) av.	1.851(2)	1.989
S−CH_2 av.	1.818(3)	1.930
B1−CH_2 av.	1.666(3)	1.651
CH_2−S−Fe av.	102.21(9)	106.20
S−C−B av.	113.97(2)	117.66
S−Fe−C22 av.	122.64(8)	122.56
C22−Fe···B	179.1	173.47

4. Discussion

The structural and spectroscopic results presented demonstrate that compound **1** is a high-spin ferrous organoiron complex. Mössbauer spectroscopy reveals that **1** has a negative zero-field splitting, $g_z > 2.00$, and uniaxial magnetic behavior, all stemming from a sizable unquenched orbital angular momentum. In the following, we use our DFT calculations to discuss the Mössbauer experimental data in the framework of ligand field theory, making correlations between the spectroscopic parameters and the molecular bonding in this novel complex.

DFT geometry optimizations and time-dependent DFT (TD-DFT) calculations were performed using the B3LYP functional and the 6-311G basis set, on three input molecular models of **1**, of which two were truncated: Model 1 replaced the *tert*-butyl substituents on each S and the phenyl substituent of B with hydrogens. Model 2 replaced the phenyl substituent on B with hydrogen. Model 3 contained all of the atoms of the full molecule, as shown in Figure 1. The agreement of the geometry optimization parameters (Table 5) with the experimental data improves significantly from the truncated to the full input structure. In particular, the Fe−C bond distances in the optimized model 1 and model 2 (2.009 and 2.018 Å, respectively) are shorter than the X-ray-derived distance of 2.034 Å, while the calculated Fe−S bonds (Fe−S_{ave} = 2.530 and 2.524 Å, respectively) are longer than the average experimental distance of 2.412 Å. In this discussion, we refer only to model 3, which yields metric parameters in reasonable agreement with those determined by X-ray crystallography (Table 5). All of the calculated metric parameters, with models 1, 2, and 3, are listed in the Supporting Information.

Zero-Field Splitting, D, and $g_{z,\text{eff}}$. The TD-DFT calculations were used to generate the relative energies of the d orbitals, as shown in Figure 6. The purpose of the DFT calculation was to try to explain the Mössbauer parameters, where possible, correlating them with geometric features and the orbital energy diagram.[40] The Mössbauer spectro-

(38) Hendrich, M. P.; Debrunner, P. G. *Biophys. J.* **1989**, *56*, 489–506.

(39) Stoian, S. A.; Smith, J. M.; Holland, P. L.; Münck, E.; Bominaar, E. L. *Inorg. Chem.* **2008**, *47*, 8687–8695.

(40) Neese, F. *J. Biol. Inorg. Chem* **2006**, *11*, 702–711.

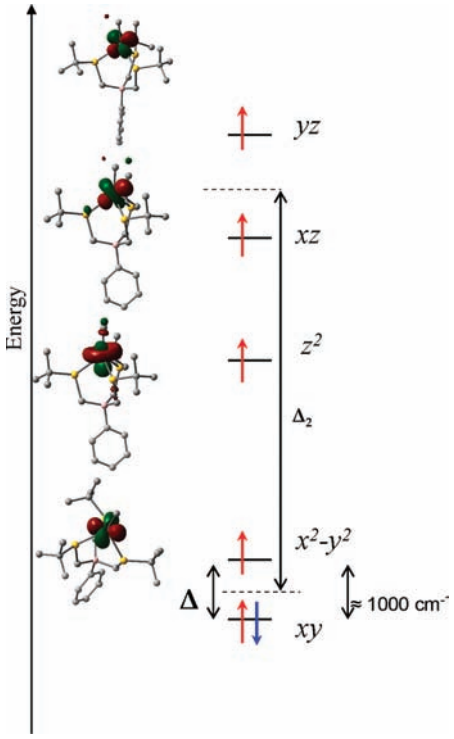

Figure 6. Qualitative sequence of the d orbitals obtained from TD-DFT calculations for **1**, and contour plots of the linear combinations of orbitals for the calculated $\beta-\beta$ transitions.

scopic parameters are calculated in the ZFS principal axis system, with the spin quantization z axis (hence, D_z) along the Fe−C axis. The TD-DFT calculations yielded a ground state overall described as $d_{xy}^2 d_{x^2-y^2}^1 d_{yz}^1 d_{xz}^1 d_{z^2}^1$, where the two lowest-lying orbitals, namely d_{xy} and $d_{x^2-y^2}$ (these orbitals are in a molecular Cartesian frame, in which the z axis was taken collinear with the Fe−C bond), are spaced by about 1300 cm^{-1}; the next excited state was at >4000 cm^{-1}. The makeup of the orbital states in an approximate C_{3v} symmetry consists of linear combinations of the d_{xy} and $d_{x^2-y^2}$ and the d_{yz} and d_{xz} functions, where the two lowest-lying states are predominantly consisting of d_{xy} and $d_{x^2-y^2}$ orbitals. Thus, the TD-DFT model generates a ground state that accounts well for the spin quantization axis, namely, the d_{xy}-like ground state, which generates a large negative ZFS on the z axis, as obtained experimentally. Assuming the limiting case of a d_{xy} ground state, and mixing by the spin−orbit coupling operator λ**LS**, we can estimate the zero-field splitting tensor components, $D_{zz} = (-4)\lambda^2/\Delta$, $D_{xx} = D_{yy} = -\lambda^2/\Delta_2$, and $g_{z,\mathrm{eff}} = [2.0 + 2(-4)\lambda]/\Delta$, yielding $D \approx -30$ cm^{-1}, $E/D = 0$, and $g_{z,\mathrm{eff}} = 2.6$,[41] where Δ is the splitting between d_{xy} and $d_{x^2-y^2}$ in Figure 6 and $\lambda = -107$ cm^{-1} is the spin−orbit coupling constant for the free high-spin ferrous ion.[42,43]

We have recorded the EPR spectra of **1** in parallel and perpendicular modes for a solid/nujol sample and a frozen toluene solution. The ZFS obtained from EPR spectra on the solution sample is in satisfactory agreement with that from fitting the Mössbauer spectra. While the toluene sample signals could be simulated well with the same species in both perpendicular and parallel modes, the solid/nujol sample presented a complex signal, composed of at least two broad species. Since the g values and ZFS parameters obtained from solution and solid-state samples are different, we considered phenomena in the solid state that could lead to broad signals. Inspection of the crystal structure reveals molecules that are separated by distances as small as 7.95 Å, ranging to 11 Å. These distances allow spin dipolar couplings in the solid of approximately 0.01 cm^{-1},[18,44] which would affect the EPR spectral shape. The angles of the Fe−C vectors of the molecules separated by 7.95 Å and 9.00 Å distances are about 40°. With these values, using eq 2, appended with the term $H_{ss} = g^2\mu_B{}^2\{(S_1\cdot S_2)/r^3 - [3(S_1\cdot \mathbf{r})(S_2\cdot \mathbf{r})]/r^5\}$ to simulate spin−spin interactions between two $S = 2$ species, with the parameters shown in Table 2, we predict that the resonance at $g = 10.2$ (approximately $B = 650$ G) would split into two resonances spaced by about 200 G. Thus, it is conceivable that dipolar couplings cause the more complex spectrum of the powder sample and contribute to the complexity observed in the low-field Mössbauer spectrum.

Table 6. Experimental and DFT Calculated Mössbauer Parameters for **1**, Derived from the Full Molecule, Model **3**

parameter	experimental	calculated
δ (mm/s)	0.6(3)	0.5
ΔE_Q (mm/s)	0.00(1)	−1.54
$A_{\mathrm{Fermi-contact}}$ (MHz)	−9	+2

Hyperfine Parameters. The 4.3 K isomer shift of $\delta = 0.6$ mm/s observed for **1** supports the assignment of the +2 oxidation state. DFT computations on all three models reproduced well the experimental value, within 0.1 mm/s (Table 6 and Table S6, Supporting Information).[45] The experimental quadrupole splitting for **1** is $\Delta E_Q = 0.00(1)$ mm/s at all temperatures. This is a surprising result for a high-spin ferrous complex with sulfur-rich coordination, since such sites typically exhibit large quadrupole splittings.[5,7,46,47] Moreover, we reported earlier the precursor complex to **1**, $\{[PhTt^{tBu}]Fe^{(II)}Cl\}_2$, which instead of the methyl contains a chloride ligand and has $\delta = 0.97$ mm/s and $\Delta E_Q = -3.32$ mm/s. The high-temperature studies in a variable magnetic field show that **1** does not develop a quadrupole splitting at high temperatures. Rather, all components of the electric field gradient are zero. DFT calculations furnished a significantly larger $\Delta E_Q(\mathrm{calcd}) = -1.54$ mm/s (Table 6). A discrepancy of similar magnitude between experimental and calculated quadrupole splittings has been reported for another trigonal-pyramidal (pseudo-C_{3v}) high-spin ferrous complex, $[PhBP^{iPr}{}_3]FeCl$ ($PhBP^{iPr}{}_3$ = $PhB(CH_2P(CH(CH_3)_2)_2)_3^-$), and is most likely due to the fact that the DFT calculations describe the ground orbital state with a single determinant.[48]

(41) Wertz, J. E.; Bolton, J. R. *Electron Spin Resonance, Elementary Theory and Practical Applications*; McGraw Hill: New York, 1972.
(42) Abragam, A.; Bleaney, B. *Electron Paramagnetic Resonanance of Transition Ions*; Clarendon Press: London, 1970.
(43) Bendix, J.; Brorson, M.; Schaffer, C. E. *Inorg. Chem.* **1993**, *32*, 2838–2849.
(44) Carlin, R. L. *Magnetochemistry*; Springer Verlag: Berlin, 1986.
(45) Neese, F. *Inorg. Chim. Acta* **2002**, *337*, 181–192.
(46) Schulz, C.; Debrunner, P. G. *J. Phys., Colloq.* **1976**, *6*, 153–8.
(47) Vrajmasu, V. V.; Bominaar, E. L.; Meyer, J.; Münck, E. *Inorg. Chem.* **2002**, *41*, 6358–6371.
(48) Hendrich, M. P.; Gunderson, W.; Behan, R. K.; Green, M. T.; Mehn, M. P.; Betley, T. A.; Lu, C. L.; Peters, J. C. *Proc. Natl. Acad. Sci. U.S.A.* **2006**, *103*, 17107–17112.

As seen above, in order to describe the zero-field splitting for **1**, the ground and first-excited states are mixed by spin−orbit coupling, which would require a linear combination of determinants for the ground state. The mixed nature of the ground orbital state may account qualitatively for the null EFGs. [A hypothetical example taking a degenerate ground state is discussed in the Supporting Information.] Ferrous sites with unusually small, but nonzero, values of the quadrupole splitting are known, albeit rare, in the literature.[3,35,48] Examples are some sterically encumbered, two- and planar three-coordinated ferrous sites in which the observed ΔE_Q was attributed to an important ligand contribution to the EFGs, opposing the ^{57}Fe valence contribution.[18] A more detailed theoretical study is necessary to establish the origins of the null EFGs of **1**.

The Mössbauer spectroscopic results show that **1** exhibits a highly anisotropic magnetic hyperfine tensor, dominated by a large orbital component. The magnetic hyperfine tensor of the ^{57}Fe nucleus is computed as the sum of three contributions, $A = A_{FC} + A_L + A_{SD}$,[42] where A_{FC} is the Fermi contact contribution (isotropic), A_L is the orbital contribution (anisotropic), and A_{SD} is the spin-dipolar contribution (traceless). From the Mössbauer spectra, we can calculate the isotropic magnetic hyperfine constant, $A_{iso}(exp) = (A_x + A_y + A_z)/3 = 35\ kG \approx 5$ MHz (containing contributions from the Fermi contact, A_{FC}, and the (orbital) pseudocontact, A_{pseudo} terms). It is important to note that, in $Fe^{(II)}S_4$ rubredoxin-type and related pseudotetrahedral ferrous sites, the orbital component of the **A** tensor is negligible, due to quenching of the orbital angular momentum by the crystal field.[41,42] Because **1** has unquenched orbital angular momentum, one must consider the orbital component in A_{iso}, known as the pseudocontact contribution, A_{pseudo}, $A_{iso} = A_{FC} + A_{pseudo}$. Since these two contributions have opposite signs, A_{iso} is small and positive.[35,47] The pseudocontact contribution is proportional to the average orbital contribution of the experimental effective **g** value, $A_{pseudo}(exp) = [(g_x + g_y + g_z)/3 - 2.00]P \approx 14$ MHz, where $P \approx 55-82$ MHz and depends on the radial expectation value $< r^{-3} >$ for d orbitals, taken here as $P \approx 68$ MHz.[42,49] Using this value, in order to obtain the very small but positive $A_{iso}(exp) \approx 5$ MHz, one must assume a Fermi contact contribution, $A_{FC} \approx -9$ MHz (called here, $A_{FC}(exp) \approx -9$ MHz), which is remarkably small compared to nonalkyl, four-coordinate ferrous sulfur-rich sites, such as rubredoxin, for which $A_{FC} = -25.8$ MHz).[47] Smaller than expected values of A_{iso} and A_{FC} have been reported for three-coordinated ferrous sites (in the M center of the MoFe protein in the nitrogenase[50] and a trigonal synthetic complex studied by Sanakis et al.).[35] Such a low Fermi contact contribution is not readily explained. The population of the 4s orbital of the iron ion could lower the contact contribution; however, this would also lead to a smaller isomer shift. While the isomer shift obtained by DFT was in good agreement with the experimental value, we cannot make quantitative theoretical predictions of A_{FC}. The DFT-calculated Fermi contact contribution is underestimated, $A_{FC}(calcd) = 2$ MHz, and it has the incorrect sign. The discrepancy in sign was unexpected since DFT-calculated isotropic contributions for other ferrous complexes have been successfully computed at the same level of theory.[51]

Conclusions

We have structurally and spectroscopically characterized a four-coordinate, sulfur-ligated organoiron complex, **1**, a high-spin ferrous species with uniaxial magnetic properties. Among the most noteworthy spectroscopic findings are a large orbital component of the magnetic hyperfine tensor, $A_z \approx +34$ MHz; the negative and of relatively large magnitude zero-field splitting, $D \approx -33\ cm^{-1}$; $g_{z,eff} \approx 2.5$; $\Delta E_Q = 0.0(1)$ mm/s; and $A_{iso} \approx 5$ MHz. The observed negative ZFS and a large orbital magnetic hyperfine component along the axis collinear with the Fe−C bond can be explained assuming a ground orbital with predominant d_{xy} character. DFT and TD-DFT calculations correctly predict the electronic ground state and the isomer shift. Further Mössbauer (and possibly, high-frequency and high-field EPR, for refinement of the fine structure parameters) and theoretical studies of this and other high-spin organoiron compounds are necessary to understand their bonding and electronic properties.

Acknowledgment. C.V.P. would like to thank Prof. Eckard Münck (Carnegie Mellon University) for the use of his Mössbauer spectrometers and laboratory and for insightful discussions; Raymond DeHont on Mössbauer spectroscopy; and Prof. Michael P. Hendrich (Carnegie Mellon University) for the free use of the Spin Count software, EPR spectrometer, and for useful suggestions and discussions. This work was in part supported by NSF grant CHE-0421116 and Faculty Development funds from Ursinus College (to C.V.P.) and NSF grants CHE-0518508 and CHE-0809603 (to C.G.R); S.A.S. was supported from grant MCB-0424494 (to Eckard Münck).

Supporting Information Available: A CIF file for **1**, additional Mössbauer simulations, the EPR spectrum of a crystalline sample of **1**, and additional details and results from DFT calculations. This material is available free of charge via the Internet at http://pubs.acs.org.

(49) Oosterhuis, W. T.; Lang, G. *Phys. Rev.* **1969**, *178*, 439–456.
(50) Yoo, S. J.; Angove, H. C.; Papaefthymiou, V.; Burgess, B. K.; Münck, E. *J. Am. Chem. Soc.* **2000**, *122*, 4926–4936.
(51) Sinnecker, S.; Slep, L. D.; Bill, E.; Neese, F. *Inorg. Chem.* **2005**, *44*, 2245–2254.
(52) Au-Yeung, H. Y.; Lam, C. H.; Lam, C.-K.; Wong, W.-Y.; Lee, H. K. *Inorg. Chem.* **2007**, *46*, 7695–7697.
(53) Bouwkamp, M. W.; Bart, S. C.; Hawrelak, E. J.; Trovitch, R. J.; Lobkovsky, E.; Chirik, P. J. *Chem. Commun.* **2005**, 3406–3408.
(54) Scott, J.; Gambarotta, S.; Korobkov, I.; Budzelaar, P. H. M. *Organometallics* **2005**, *24*, 6298–6300.
(55) Fürstner, A.; Martin, R.; Krause, H.; Seidel, G.; Goddard, R.; Lehmann, C. W. *J. Am. Chem. Soc.* **2008**, *130*, 8773–8787.